Finite element computation of the electromechanical J-Integral for 2–D and 3–D crack analysis

M. Abendroth*, U. Groh, M. Kuna and A. Ricoeur
Freiberg University of Mining and Technology
Institute of Mechanics and Fluid Dynamics
Lampadiusstraße 4, D-09596 Freiberg, Germany

Abstract. Piezoelectric ceramics find an application in many fields of technology. They may serve as sensors or actuators, mostly beeing exposed to high electric and mechanical loads. Therefore, fracture mechanics of piezoelectrics is an important field preserving strength and reliability under different conditions of application.

This paper deals with the calculation of electromechanical energy release rates for arbitrary cracks in spatial piezoelectric structures applying a generalized J–integral. The crack problem is solved using a commercial FEM-code obtaining electric and mechanical field variables in nodes and integration points. These results serve as input data for the numerical computation of the electromechanical J–integral. The results are compared to findings from analytical and alternative numerical methods.

Keywords: J–integral, fracture mechanics, finite element method, piezoelectricity, brittle fracture, ceramics

1. Introduction

Multi functional materials such as piezoelectric ceramics are gaining growing interest for the development of electromechanical systems, recently applied in electronics, micro system technology, mechatronics or adaptive structures. The integration of these smart materials into structural components supplies the essential sensing and actuating functionality. As a consequence, these smart materials may be exposed to extraordinary high mechanical and electric static, dynamic or cyclic loading. Thus, besides their functional features improved mechanical properties are required as well. Therefore, problems of strength, fracture and fatigue of the involved smart electroceramics arise. They play an important role for the optimum design and the reliable performance of electromechanical systems and devices. The macroscopic failure of piezoelectric ceramics is mainly determined by the growth of microscopic cracks. Here, mechanical and electric intensity factors and energy release rates play an important role as fracture quantities.

This paper presents an efficient method for the numerical implementation of the J–integral yielding electromechanical energy release rates.

* Martin.Abendroth@imfd.tu-freiberg.de

In contrast with recent papers [8, 10], our work is focussed on cracks in 3–dimensional (3–D) piezoelectric structures with arbitrary shaped crack fronts. J–integral calculations of spatial crack configurations have been restricted to mechanical [7, 12, 19] or thermo–mechanical problems, yet [5, 18].

Starting from the well known classical J–integral by Rice [16] and Cherepanov [4], the theory of the J–integral in coupled electromechanical fields goes back to Pak [13, 14] and has been further generalized by Kuna [9–11], accounting for volume forces and charges, as well as tractions and charges at the crack faces and heterogenous structures.

All calculations are based on field results obtained by the finite element code ABAQUS [1]. In a first step, the boundary value problem of an arbitrary crack front configuration in a piezoelectric structure is solved under electromechanical loading conditions. The results for nodal potentials and displacements, such as stresses and electric displacements in the integration points are subsequently included in the calculation of the J–integral.

2. Electromechanical fracture mechanics

The principles of electromechanical fracture mechanics have been generalized to anisotropic piezoelectric media within a linear theory by several workers e.g. Suo at al. [20], Pak [13, 14], Park and Sun [15]. The basic relations used in the following sections originate from these works.

2.1. The piezoelectric continuum

The mathematical description of the piezoelectric continuum is governed by the equations of linear electro– and elastostatics. The mechanical strain tensor ε_{ij} is deduced from the mechanical displacement vector u_i by the gradient operation

$$\varepsilon_{ij} = \frac{1}{2}\left(u_{i,j} + u_{j,i}\right). \tag{1}$$

In electrostatics the electric potential φ is the field variable corresponding to the mechanical displacements, thus the electric field vector E_k is also obtained by the differentiation

$$E_k = -\varphi_{,k}. \tag{2}$$

The balance equations in the domain V for the mechanical forces and the electric charges are

$$\sigma_{ij,j} + b_i = 0, \tag{3}$$

$$D_{i,i} - \omega_V = 0. \tag{4}$$

At the boundary S of the domain V, one has to prescribe either the primary variables u_i and/or φ or the tractions T_i and/or the surface charges ω_S

$$\sigma_{ij} n_j = T_i, \tag{5}$$

$$D_j n_j = -\omega_S. \tag{6}$$

Here σ_{ij} denotes the stress tensor, D_i the electric flux density, b_i the volume forces, ω_V the volume charges, T_i the boundary tractions, ω_S the surface charge density and n_j the normal vector at the domain boundary.

The mechanical and electric fields are coupled by constitutive equations. Eqn. (7) describes the indirect or actoric piezoelectric effect and Eqn. (8) describes the direct or sensoric effect. The material properties are determined by the elastic constants C_{ijkl}, the piezoelectric constants e_{ikl} and the dielectric constants κ_{ij}.

$$\sigma_{ij} = C_{ijkl}\varepsilon_{kl} - e_{mij}E_m = \frac{\partial H}{\partial \varepsilon_{ij}} \tag{7}$$

$$D_n = e_{nkl}\varepsilon_{kl} + \kappa_{nm}E_m = -\frac{\partial H}{\partial E_n} \tag{8}$$

According to thermodynamics, these relations can also be deduced by differentiation of the electric enthalpy density H with respect to state variables ε_{ij} and E_n. The field variable H is defined as

$$H(\varepsilon_{ik}, E_i) = \frac{1}{2} C_{ijkl}\varepsilon_{ij}\varepsilon_{kl} - e_{ikl}E_i\varepsilon_{kl} - \frac{1}{2}\kappa_{ij}E_iE_j. \tag{9}$$

Because of the symmetry of the material tensors and furthermore accounting for the constitutive equations (7) and (8), Eqn. (9) can be reduced to

$$H = \frac{1}{2}\left(\sigma_{ij}\varepsilon_{ij} - D_iE_i\right). \tag{10}$$

2.2. The 2–dimensional electromechanical J–Integral

We focus our attention on a domain V, which is part of a piezoelectric continuum and surrounded by a closed path S, see Fig. 1. According to works from Eshelby [6] and Rice [16] for pure mechanical applications we write

$$F_k = \oint_S \left(H\delta_{kj} - \sigma_{ij}u_{i,k} + D_jE_k\right) n_j \, ds. \tag{11}$$

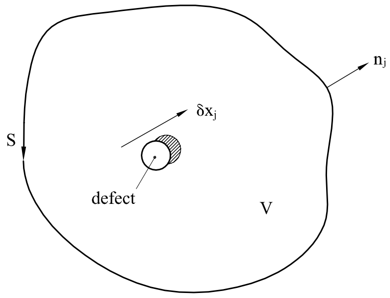

Figure 1. Closed integration path around a defect

Eqn. (11) describes the material force, if an electromechanically loaded domain is virtually displaced by the vector δx_k. The term in brackets is called the piezoelectric energy momentum tensor

$$Q_{kj} = H\delta_{kj} - \sigma_{ij}u_{i,k} + D_j E_k \tag{12}$$

analogous to the energy momentum tensor, which was introduced by Eshelby [6]. If the integration path S contains neither defects nor source terms b_i and ω_V, then the force vanishes and $F_k \equiv 0$. Now we consider a path Γ_ε enclosing the tip of a crack, see Fig. 2. The electromechanical J_k^{em}–integral vector is the material force associated with the crack tip singularity. It is defined as the limit, if Γ_ε is shrunk towards $r \to 0$

$$J_k^{em} = \lim_{r\to 0} \int\limits_{\Gamma_\varepsilon} Q_{kj} n_j \, ds = \lim_{r\to 0} \int\limits_{\Gamma_\varepsilon} \left(H\delta_{kj} - \sigma_{ij}u_{i,k} + D_j E_k\right) n_j \, ds. \tag{13}$$

To discuss the path dependence of J_k^{em}, a closed integration path $S = \Gamma - \Gamma_\varepsilon + \Gamma^+ + \Gamma^-$ is constructed, which surrounds the homogeneous domain V but excludes the crack tip. Because V is free of defects and source terms, the integral Eqn. (11) over S is zero, i. e. we find with Eqn. (13)

$$\begin{aligned} J_k^{em} &= \lim_{r\to 0} \int\limits_{\Gamma+\Gamma^+ +\Gamma^-} Q_{kj} n_j \, ds \\ &= \int\limits_{\Gamma} Q_{kj} n_j \, ds + \lim_{r\to 0} \int\limits_{\Gamma^+ +\Gamma^-} Q_{kj} n_j \, ds. \end{aligned} \tag{14}$$

From here one can conclude that the evaluation of the J_k^{em}–integral gives the same value for any arbitrary path Γ, if the second term of Eqn. (14) vanishes, i. e.

$$\lim_{r\to 0} \int\limits_{\Gamma^+ +\Gamma^-} (H n_k - \underbrace{\sigma_{ij} n_j}_{T_i} u_{i,k} + \underbrace{D_j n_j}_{-\omega_S} E_k) ds \overset{!}{=} 0. \tag{15}$$

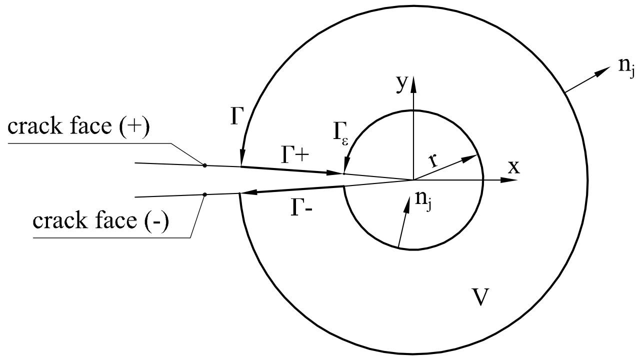

Figure 2. Combined integration path around a cracktip

Let us assume an electrically impermeable crack, which implies the boundary conditions $D_j n_j = -\omega_S$ for the crack. Then it is neccessary to satisfy Eqn. (15) that the tractions and charges are zero on the crack faces Γ^+ and Γ^-

$$T_i \equiv 0\,, \quad \omega_S \equiv 0. \tag{16}$$

If straight crack faces with the normal vector in y–direction are presupposed, i. e. $n_k = \mp\delta_{2k}$ on Γ^+ an Γ^-, the first term in Eqn. (15) reduces to $(H^- - H^+)\delta_{2k}$. From Eqn. (14) follows

$$\begin{aligned} J_k^{em} &= \int\limits_{\Gamma} \left(H\delta_{kj} - \sigma_{ij}u_{i,k} + D_j E_k\right) n_j \, ds \\ &+ \lim_{r\to 0} \int\limits_{\Gamma+} \left(H^- - H^+\right) \delta_{2k} \, ds. \end{aligned} \tag{17}$$

Therefore, the evaluation of J_k^{em} is independent of the integration path Γ for the component $k = 1$ and also for $k = 2$, if the enthalpy density H^+ and H^- at the crack faces is considered.

J_k^{em} denotes the electromechanical J–integral vector. For $k = 1$ the energy release rate $J_1^{em} = G$ is obtained. If electric contributions are neglected, i. e. $D_j E_k = 0$ in Eqns. (11...13) and $D_i E_i = 0$ in Eqn. (10) the classical J–integral derived by Rice [16] and Cherepanov [4] is obtained.

2.2.1. *Transformation into an equivalent domain integral*

For the numerical analysis of the J_k^{em}–integral an equivalent domain integral is easier to handle than a line integral. The condition for the transformation into a domain integral applying the Gaussian integral theorem, a closed integration path S with an outward pointing normal vector is given, as can be seen in Fig. 2. Instead of Eqn. (13) and with respect to path independence we write

$$J_k^{em} = -\int\limits_S Q_{kj} n_j \, ds + \int\limits_{\Gamma+\Gamma^+ +\Gamma^-} Q_{kj} n_j \, ds. \tag{18}$$

Now a weighting function q is introduced, which should be continuous and satisfy the condition

$$q = \begin{cases} 0 & \text{on} \quad \Gamma \\ 1 & \text{on} \quad \Gamma_\varepsilon \end{cases} . \tag{19}$$

If the weighting function q is introduced into Eqn. (18), the contribution of the integral along Γ disappears and

$$J_k^{em} = -\int\limits_S Q_{kj} n_j q \, ds + \int\limits_{\Gamma^+ +\Gamma^-} Q_{kj} n_j q \, ds. \tag{20}$$

The transformation into an equivalent domain integral leads to

$$J_k^{em} = -\int\limits_V (Q_{kj} q)_{,j} \, dV + \int\limits_{\Gamma^+ +\Gamma^-} Q_{kj} n_j q \, ds. \tag{21}$$

If we use the whole expression for Q_{kj} from Eqn. (12) we get the 2–dimensional J_k^{em}–integral as a domain integral

$$\begin{aligned} J_k^{em} \;=\; & -\int\limits_V (H\delta_{kj} - \sigma_{ij} u_{i,k} + D_j E_k) \, q_{,j} \, dV \\ & -\int\limits_V \Big(H_{,k}\big|_{exp} + b_i u_{i,k} + \omega_V E_k \Big) \, q \, dV \qquad (22) \\ & + \int\limits_{\Gamma^+ +\Gamma^-} (H n_k - T_i u_{i,k} - \omega_S E_k) \, q \, ds. \qquad (23) \end{aligned}$$

If the material is homogenous, no volume forces or charges and no crack face tractions or charges are applied and if the crack face normals point into the y–direction, i. e.

$$\begin{aligned} & H_{,k}\big|_{exp} = 0, \\ & b_i = 0, \quad \omega_V = 0, \\ & T_i = 0, \quad \omega_S = 0, \\ & n_k = (0, \; \pm 1)^T \end{aligned} \tag{24}$$

Eqn. (23) can be reduced to

$$J_k^{em} = -\int\limits_V (H\delta_{kj} - \sigma_{ij} u_{i,k} + D_j E_k) \, q_{,j} \, dV + \int\limits_{\Gamma^+ +\Gamma^-} (H n_k) \, q \, ds. \tag{25}$$

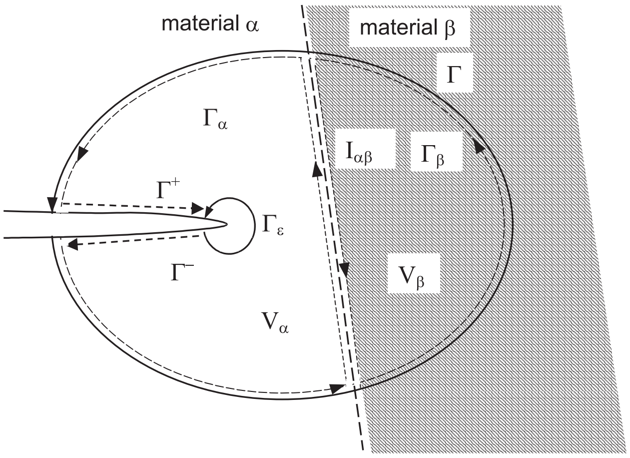

Figure 3. Domain of integration for a crack in a heterogeneous structure

2.3. Extension of J_k^{em} for cracks in heterogeneous structures

The J_k^{em}–integral is evaluated for the case that the cracked structure contains regions with dissimilar materials, e.g. compound materials or phase boundaries as shown in Fig. 3. At an interface $I_{\alpha\beta}$ between two dissimilar material pairs α and β, the elastic, piezoelectric and dielectric material properties are changing discontinuously. The displacements and the electric potential are continuous at the interface:

$$u_i^{(\alpha)} = u_i^{(\beta)} \tag{26}$$

$$\varphi^{(\alpha)} = \varphi^{(\beta)} \tag{27}$$

If no external forces or charges act in the interface, the reciprocity conditions hold for the mechanical tractions T_i and the electric surface charges ω_S at the interface:

$$T_i^{(\alpha)} + T_i^{(\beta)} = \left(\sigma_{ij}^{(\alpha)} - \sigma_{ij}^{(\beta)}\right) n_j^{(\alpha)} = 0 \tag{28}$$

$$\omega_S^{(\alpha)} + \omega_S^{(\beta)} = -\left(D_j^{(\alpha)} - D_j^{(\beta)}\right) n_j^{(\alpha)} = 0 \tag{29}$$

Invoking the virtual work principle for the interface, the materials force F_k acting on the interface could be derived in [9]. It is computed as a line integral along the interface $I_{\alpha\beta}$ enclosed in the integration domain

V:

$$
\begin{aligned}
F_k &= -\oint\limits_{I_{\alpha\beta}} \left(Q_{kj}^{(\beta)} - Q_{kj}^{(\alpha)}\right) n_j^{(\alpha)}\, ds \\
&= \oint\limits_{I_{\alpha\beta}} \left\{ [u_{i,k}]_\alpha^\beta\, \sigma_{ij}^\alpha n_j^\alpha + [\varphi_{,k}]_\alpha^\beta\, D_j^{(\alpha)} n_j^{(\alpha)} - [H]_\alpha^\beta\, n_k^{(\alpha)} \right\} ds \qquad (30)
\end{aligned}
$$

Expressions in brackets $[a]_\alpha^\beta = a^{(\beta)} - a^{(\alpha)}$ denote the jump of a quantity a at the phase boundary between two material regions (α) and (β). The same result is obtained, if one decomposes the total J_k^{em}–integration path Γ into two separate integrals along the material regions Γ_α and Γ_β, see Fig. 3.

Using this result, the J_k^{em}–integral can be extended for a crack in an arbitrary heterogenous structure, composed from M dissimilar material regions V_α with corresponding interface pairs $I_{\alpha\beta}$ with $\alpha, \beta = 1, 2, \ldots M$. Furthermore, the material properties may vary smoothly within each region V_α.

$$
\begin{aligned}
J_k^{em} &= \int\limits_\Gamma \left(H\delta_{kj} - \sigma_{ij} u_{i,k} + D_j E_k\right) n_j\, ds \\
&- \int\limits_{\Gamma^+ + \Gamma^-} \left(T_i u_{i,k} + \omega_S E_k - H n_2 \delta_{2k}\right) ds \\
&- \sum_{\alpha,\,\beta} \int\limits_{I_{\alpha\beta}} \left\{ [u_{i,k}]_\alpha^\beta\, \sigma_{ij}^{(\alpha)} n_j^{(\alpha)} + [\varphi_{,k}]_\alpha^\beta\, D_j^{(\alpha)} n_j^{(\alpha)} - [H]_\alpha^\beta\, n_k^{(\alpha)} \right\} ds \\
&- \sum_{\alpha=1}^{M} \int\limits_{V_\alpha} \left(b_i u_{i,k} + \omega_V E_k + H_{,k}|_{exp}\right) dV \qquad (31)
\end{aligned}
$$

With Eqn. (31) one can determine the electromechanical energy release rate of a crack in a complex heterogeneous piezoelectric structure under quite general electric and mechanical loading at the crack faces and in the volume. It allows to treat jump–like material changes, occurring at phase boundaries, as well as continous local variation of the piezoelectric, elastic and dielectric properties within every material region. It can be shown [9] that this integral is independent of the choice of the integration path Γ.

2.4. The 3–dimensional electromechanical J–Integral

In the 3–dimensional case a local coordinate system on the crack front is defined with the x–axis pointing normal to the crack front. The y–axis

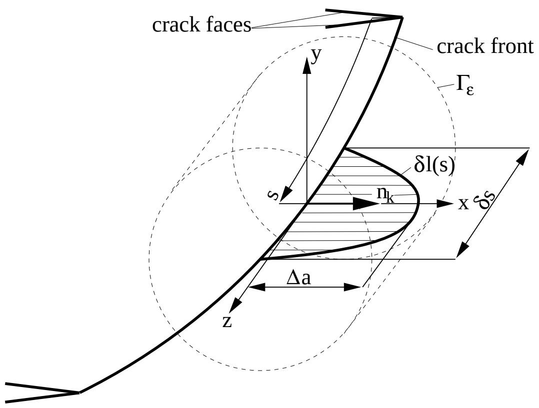

Figure 4. Arbitrary 3–dimensional crack front with a virtual crack front extension

points normal to the crack faces and the z–axis is pointing tangential to the crack front (see Fig. 4). At the position s of the crack front a virtual crack front extension $\delta l(s)$ is defined, which lies in the zx–plane. δs is the arclength of the corresponding crack front segment and Δa defines the maximum crack advance along δs. Under these conditions the averaged released energy $\delta\Pi$ along δs with respect to the crack extension Δa is

$$-\delta\Pi = \bar{J}^{em}\Delta a = \int_{\delta s} J^{em}(s)\delta l(s)\, ds. \tag{32}$$

With the vector of the virtual crack advance in x_k–direction l_k $(0 < |l_k| < 1)$ we find for the virtual crack front extension

$$\delta l(s) = \Delta a\, l_k n_k, \tag{33}$$

where n_k is the vector normal to the crack front lying in the zx–plane. Inserting Eqn. (33) into Eqn. (32) leads to

$$\bar{J}^{em} = \int_{\delta s} J^{em}(s) l_k n_k\, ds. \tag{34}$$

Considering the relation

$$J^{em}(s) n_k = J_k^{em} \tag{35}$$

Eqn. (13) can be inserted into Eqn. (34) yielding

$$\bar{J}^{em} = \int_{\delta s} l_k \left(\lim_{\Gamma_\varepsilon \to 0} \int_{\Gamma_\varepsilon} Q_{kj} n_j\, d\Gamma \right) ds. \tag{36}$$

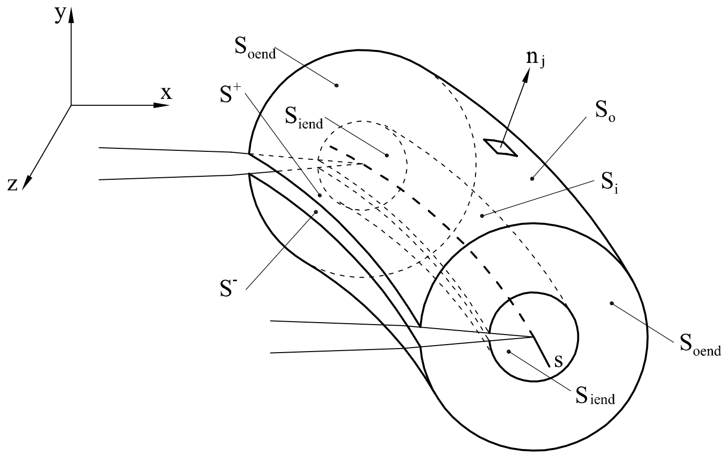

Figure 5. Integration volume with the boundaries for 3–dimensional J–Integral

The boundary Γ_ε and the arclength δs are merged into the surface S.

$$\bar{J}^{em} = \int_S Q_{kj} l_k n_j \, dA \tag{37}$$

Because of Eqn. (35), the 3–dimensional J–integral is a scalar and not a vector like the 2–dimensional formulation.

To calculate the local energy release rate $J^{em}(s)$, the following simplification is done according to [5]. $J^{em}(s)$ in Eqn. (34) is taken outside the integral and we find

$$J^{em}(s) = \frac{\bar{J}^{em}}{\int_{\delta s} l_k n_k \, ds}. \tag{38}$$

2.4.1. *Transformation into an equivalent domain integral*

The integral in Eqn. (37) should be transformed into an equivalent domain integral to improve the numerical determination. Fig. 5 supplies a closer look to the integration domain emphasized in Fig. 4 by the dashed contour. The transformation into an equivalent domain integral again requires the introduction of a weighting function, which is a vector

$$q_k = \begin{cases} 0 & \text{on} \quad S_o, S_{oend} \\ l_k & \text{on} \quad S_i, S_{iend} \end{cases} \tag{39}$$

in the 3–dimensional case. Then, the general 3–dimensional electromechanical J–Integral as a domain integral formulation is

$$\bar{J}^{em} = -\int_V \left(H\delta_{kj} - \sigma_{ij} u_{i,k} + D_j E_k \right) q_{k,j} \, dV$$

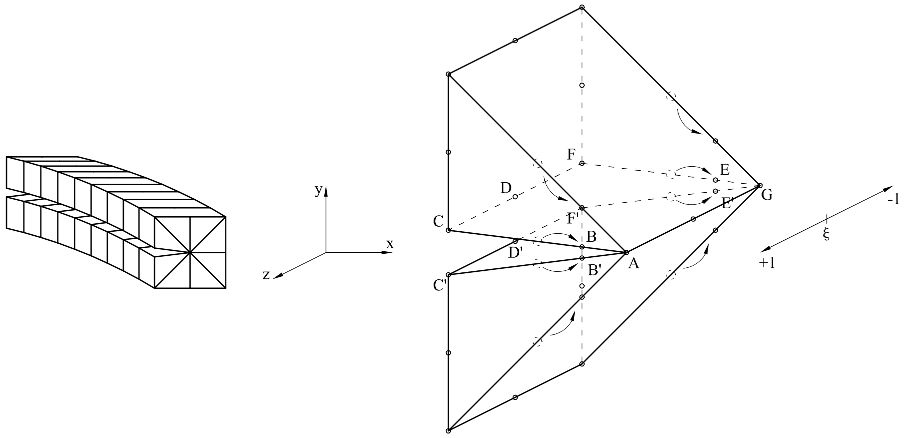

Figure 6. Meshed crack front with crack tip elements

$$- \int\limits_V \left(H_{,k}|_{exp} + b_i u_{i,k} + \omega_V E_k \right) q_k \, dV \tag{40}$$

$$+ \int\limits_{S^+ + S^-} \left(H n_k - T_i u_{i,k} - \omega_S E_k \right) q_k \, dA. \tag{41}$$

With the same restrictions as described in Eqns. (24), Eqn. (40) reduces to

$$\bar{J}^{em} = - \int\limits_V \left(H \delta_{kj} - \sigma_{ij} u_{i,k} + D_j E_k \right) q_{k,j} \, dV, \tag{42}$$

if the vector l_k lies in the zx–plane, thus $l_k n_k$ on the crack faces S^+ and S^- is zero.

The numerical integration of Eqn. (42) is used to calculate the electromechanical energy release rate for a piezoceramic structure with a crack. It should be pointed out that Eqn. (42) is valid only for an impermeable crack. The function q_k can be seen as a unit virtual displacement for all points on the contour Γ_ε in Fig. 4. Therefore this method can be interpreted as a virtual crack extension technique.

2.5. Singular electromechanical crack tip elements

Special **C**rack **T**ip **E**lements (CTE-method) are developed by modifying the shape functions of isoparametric hexaeder elements in order to account for the proper $1/\sqrt{r}$–field singularities at the crack front. By means of this method, stress intensity factors K_I, K_{II} and K_{III} as well as an electric intensity factor K_{IV}, describing the $1/\sqrt{r}$–behavior of the electric displacement, are calculated. The results are used for comparison with the J–integral calculations. Here, just a brief description of the method is given, a more detailed insight can be found in [11]. To account for the field singularities at the crack front, some element nodes are shifted from a mid-side position to the 1/4–position, see Fig. 6. Furthermore, one element face is collapsed, transforming the hexaeder element into a pentahedron element. In this paper we will call these elements quarter point elements. The intensity factors

$$\mathbf{K}(\xi) = \sqrt{\frac{\pi}{8L}}\mathbf{Y}^{-1}\left(\mathbf{a} + \frac{1}{2}\xi\mathbf{b} + \xi^2\mathbf{c}\right) \tag{43}$$

where

$$\begin{aligned} \mathbf{a} &= 2\mathbf{u}_B - \mathbf{u}_C + 2\mathbf{u}_E - \mathbf{u}_F + \mathbf{u}_D - 2\mathbf{u}_{B'} + \mathbf{u}_{C'} - 2\mathbf{u}_{E'} + \mathbf{u}_{F'} - \mathbf{u}_{D'} \\ \mathbf{b} &= -4\mathbf{u}_B + \mathbf{u}_C + 4\mathbf{u}_E - \mathbf{u}_F + 4\mathbf{u}_{B'} - \mathbf{u}_{C'} - 4\mathbf{u}_{E'} + \mathbf{u}_{F'} \\ \mathbf{c} &= \mathbf{u}_F + \mathbf{u}_C - 2\mathbf{u}_D - \mathbf{u}_{F'} - \mathbf{u}_{C'} + 2\mathbf{u}_{D'} \end{aligned} \tag{44}$$

are calculated from the vector $\mathbf{u}$ including the mechanical diplacements u_i and the electric potentials φ of the indicated node, see Eqn. (46), as well as the inverse of the Irwin matrix $\mathbf{Y}$, which is presented in Eqn. (47) for the case of a poling perpendicular to the crack faces. L defines the length of element edges containing a 1/4–point node.

$$\mathbf{K}(\xi) = [K_{II},\, K_I,\, K_{III},\, K_{IV}]^T \tag{45}$$

$$\mathbf{u} = [u_x,\, u_y,\, u_z,\, \varphi]^T \tag{46}$$

$$\mathbf{Y}^{-1} = \begin{bmatrix} c_L & 0 & 0 & 0 \\ 0 & \frac{c_T e^2}{c_T\kappa + e^2} & 0 & \frac{c_T e\kappa}{c_T\kappa + e^2} \\ 0 & 0 & c_A & 0 \\ 0 & \frac{c_T e\kappa}{c_T\kappa + e^2} & 0 & \frac{-e^2\kappa}{c_T\kappa + e^2} \end{bmatrix} \tag{47}$$

c_L, c_T, c_A, e und κ are effective material constants calculated from an analytical solution of the piezoelectric crack problem [14]. An advantage of the CTE-method is the possibility to calculate the mechanical and electric energy release rates separately. Intensity factors and the energy release rate are related by

$$G = \frac{1}{2}\mathbf{K}^T\mathbf{Y}\mathbf{K} \tag{48}$$

For the special case of a material poled perpendicular to the crack faces, the mechanical and electric energy release rates G^m and G^e are

$$\begin{aligned} G^{em} = G^m + G^e &= \frac{1}{2}\left(\frac{K_I^2}{c_T} + \frac{K_{II}^2}{c_L} + \frac{K_{III}^2}{c_A} + \frac{K_I K_{IV}}{e}\right) \\ &+ \frac{1}{2}\left(\frac{K_I K_{IV}}{e} - \frac{K_{IV}^2}{\kappa}\right) \end{aligned} \tag{49}$$

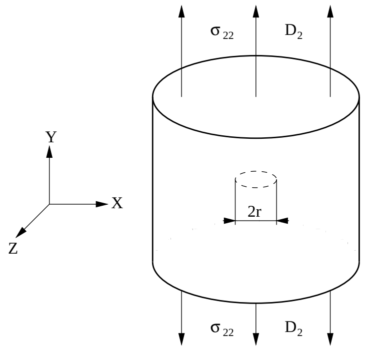

Figure 7. Penny shaped crack under combined mechanical and electric loadings

2.6. Analytical solution for a penny shaped crack

For a penny shaped crack in an infinite domain, see Fig. 7, the following solutions for K_I and K_{IV} have been found in [3]:

$$K_I = 2\sqrt{\frac{r}{\pi}}\sigma_{22}^{\infty} \tag{50}$$

$$K_{IV} = 2\sqrt{\frac{r}{\pi}}D_2^{\infty} \tag{51}$$

Here, r is the radius of the crack, σ_{22}^{∞} is the mechanical stress and D_2^{∞} is the electric displacement at infinity, respectively.

3. Numerical discretization of the J-Integral

Here we will focus on Eqn. (42), which was derived in section 2.4. The numerical integration of a physical field variable F over a domain requires the summation over all its values $F^{(ip)}$ at specific integration points multiplied by their weighting value $w^{(ip)}$ for all elements belonging to the domain.

$$\bar{J}^{em}_{num} = \sum_{elements}\sum_{ips} F^{(ip)} w^{(ip)} \left|\mathbf{J}^{(ip)}\right| \tag{52}$$

$\mathbf{J}^{(ip)}$ denotes the Jacobian matrix of the transformation between the global (x, y, z) and the local element (r, s, t) coordinate system, i. e. $dx\,dy\,dz = \left|\mathbf{J}^{(ip)}\right| dr\,ds\,dt$. In our case the field variable is the integrand of Eqn. (42), which can be written for a single integration point (ip) as

$$F^{(ip)} = \left(H^{(ip)}\delta_{kj} - \sigma_{ij}^{(ip)}u_{i,k}^{(ip)} + D_j^{(ip)}E_k^{(ip)}\right) q_{k,j}^{(ip)}. \tag{53}$$

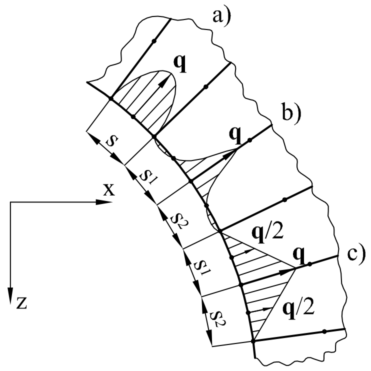

Figure 8. Defining q_i on crack front elements

Inserting Eqn. (53) into Eqn. (52) gives

$$\bar{J}^{em}_{num} = \sum_{elements} \sum_{ips} F^{(ip)} \left| \mathbf{J}^{(ip)} \right| w^{(ip)}. \tag{54}$$

To calculate $\bar{J}^{em}_{num}$ according to Eqn. (54), the values of all field variables in the integration points have to be determined from the finite element results. The stresses σ_{ij}, electric fields E_k and the electric displacements D_j are directly available at the integration points. The values of the displacements u_i are known in the nodes of the elements and have to be calculated in the integration points. In section 3.1 the weighting function q_k will be defined in the nodes and therefore it has to be calculated in the integration points as well. Using the shape functions $h^\alpha(r_i)$, of a 20–node isoparametric element we find for the gradient

$$q_{k,j} = \mathbf{J^{-1}} \sum_{\alpha=1}^{20} \frac{\partial h^\alpha}{\partial r_j} q_k^\alpha. \tag{55}$$

3.1. The weighting function q

The J-integral method for calculating the energy release rate can be interpreted as virtual crack extension method. The vector of the weighting function q_i, which was introduced in section 2.4, defines the virtual crack front extension, which may be of arbitrary shape. For a finite element mesh, q_i refers to nodes, that belong to crack front elements. Fig. 8 shows three suitable possibilities for defining a crack front extension. The shifted nodes can be *a*) a middle node of an element edge or *b*) a corner node of an element. A combination of *a*) and *b*) leads to *c*), where on a corner node q_i and on the adjacent middle nodes $q_i/2$ is applied. The shape of these resulting crack front extensions depends

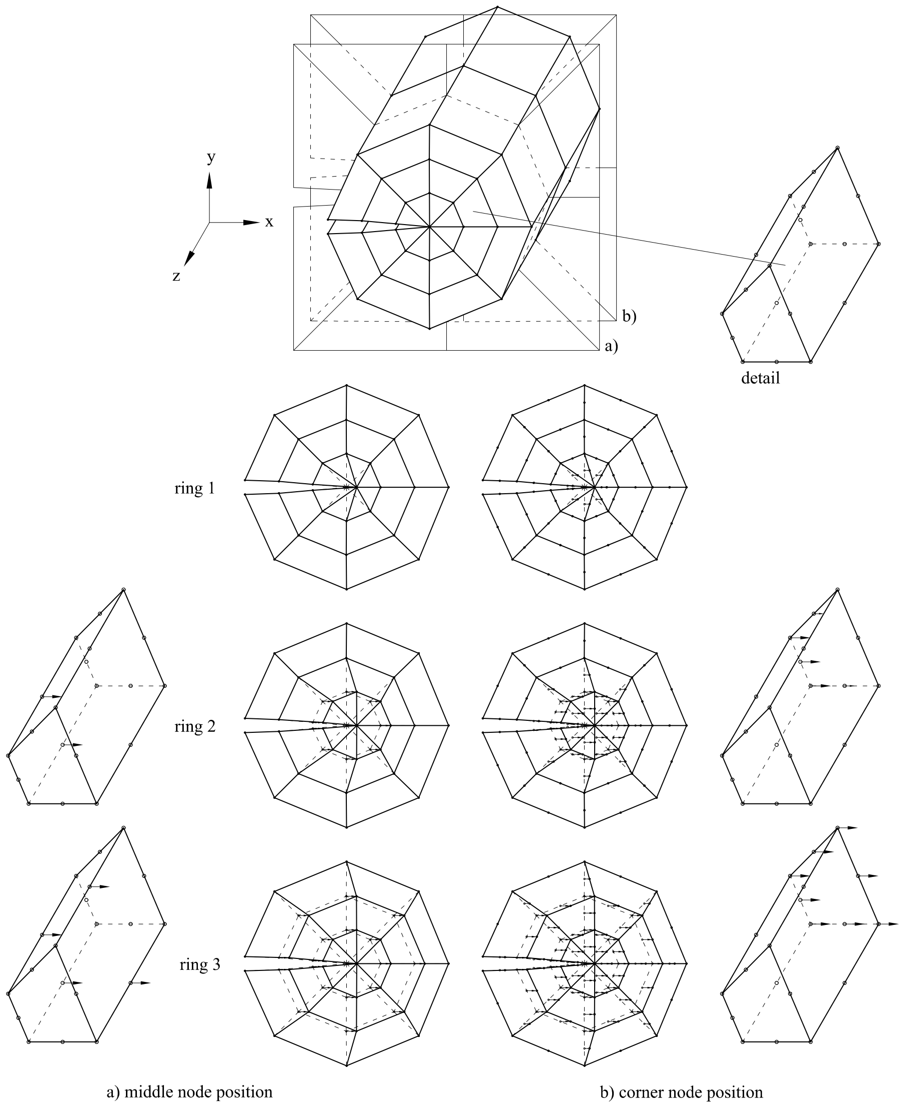

Figure 9. Definition of **q** on different postions of the crack front

on the shape functions of the elements. The isoparametric 20–node brick elements have quadratic shape functions and so the function q_i is quadratic as well. Fig. 9 shows the distribution of shifted nodes within a 3–dimensional mesh. Since the gradient $q_{i,j}$ does not vanish for interior rings, the numerical integration according to Eqn. (54) always has to be performed starting with the ring closest to the crack front.

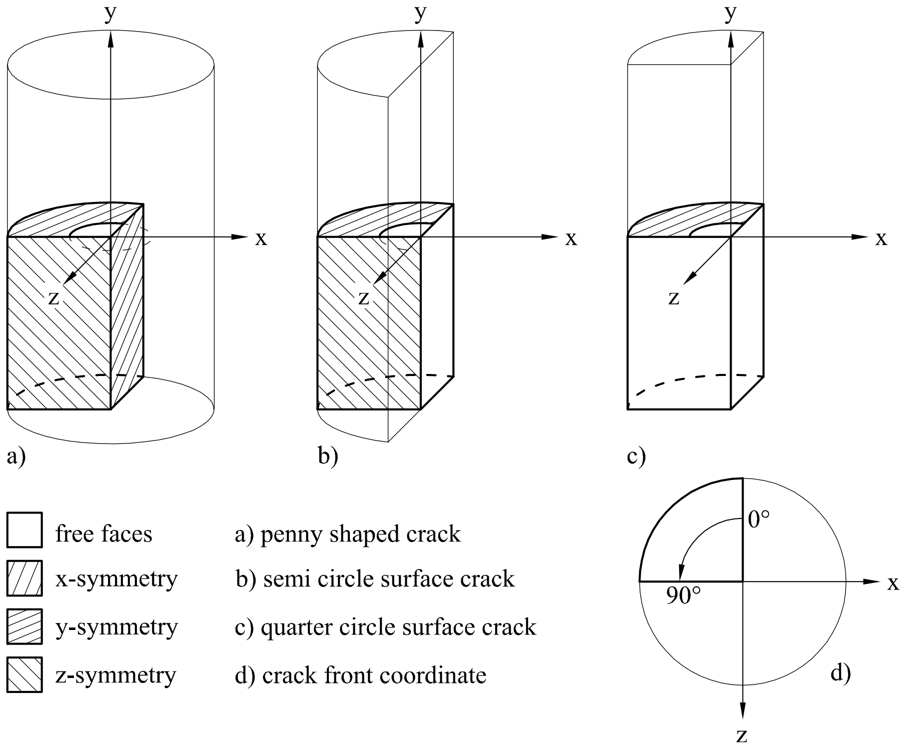

Figure 10. Symmetries on the penny shaped crack model

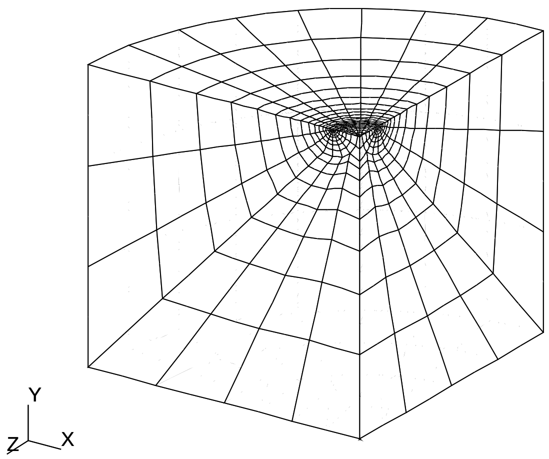

Figure 11. FE-mesh for the penny shaped crack model

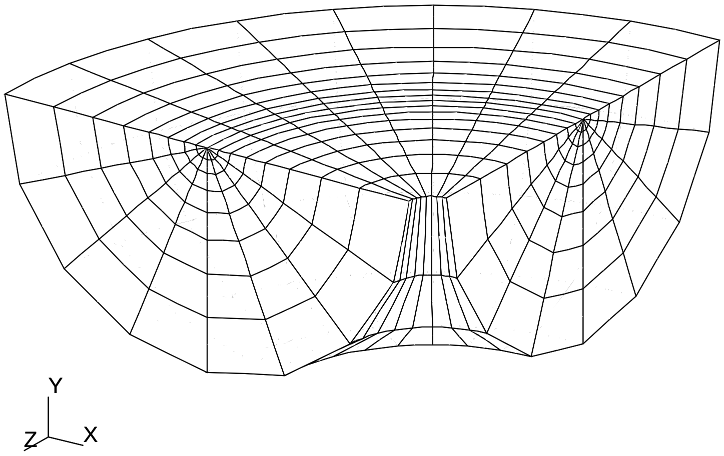

Figure 12. Detail of the surrounding region of the crack front

4. FE–model of the penny shaped crack

The model of a penny shaped crack in an infinite domain, see Fig. 7, can be realized in an FEM–model if the geometric relation between the outer dimensions and the crack dimensions are sufficiently large. A proportion of $R : r = 10 : 1$ would fit the requirements, if R is the outer radius of the model and r is the crack radius. The model has three symmetry planes, the reason why a $\frac{1}{8}$–model shown in Fig. 10 is sufficient. If the symmetry in z–direction is not used, the model becomes a semi cylinder with a semi circular surface crack. A quarter cylinder model is possible, if the symmetries in x– and z–direction are not used. Fig. 11 shows the mesh for the $\frac{1}{8}$–model and Fig. 12 presents a detail of the region surrounding the crack front. The crack tip elements are quarter point elements, introduced in section 2.5. The mesh structure around the crack front consists of layers of concentric semi rings, whereby each semi ring consists of 8 elements. To realize the geometric symmetries, displacement boundary conditions have to be applied. All nodes of a symmetry plane are fixed in the normal direction of the respective symmetry plane. Additionally, there is an electric symmetry in y–direction, that means all nodes of the y–symmetry plane have an electric potential of zero. To apply mechanical and electric loads to the model, a pressure ($\sigma_{22} = 1\,MPa$) and/or an electric flux ($D_2 = 0.001\,C/m^2$) are applied to all element faces belonging to the free surface with the normal pointing in negative y–direction.

Table I. Comparison of numerical results in 2D-case

	Loads: $\sigma_{22} = 10\,MPa$, $D_2 = 0.001\,C/m^2$		
	mechanical	electrical	electromechanical
Number of element rings	Electromechanical J-integral J_1^{em} $\left[\frac{N}{m}\right]$		
1	2487.3	−69.495	2806.1
2	2588.1	−72.337	2919.9
3	2589.9	−72.364	2921.8
4	2590.0	−72.368	2922.0
5	2590.1	−72.369	2922.0
6	2590.1	−72.369	2922.0
7	2590.1	−72.369	2922.0
8	2590.1	−72.369	2922.1
9	2590.1	−72.369	2922.1
10	2590.1	−72.369	2922.1
11	2590.1	−72.369	2922.1
12	2590.1	−72.369	2922.1
13	2590.1	−72.369	2922.0
14	2590.0	−72.368	2922.0
	Energy release rate G^{em} $\left[\frac{N}{m}\right]$ by modified crack closure integral		
	2590.0	−72.291	2920.7
	Energy release rate G^{em} $\left[\frac{N}{m}\right]$ by analytical solution [14]		
	2523.6	−71.910	2853.0

5. Results

In a first step the corresponding 2–D problem (Griffith crack) is used to compare the energy release rates calculated by the 2–D version of the prescribed algorithm for J_k^{em} with the values G^{em} received from the modified crack closure integral method [11] on the same FEM mesh. The material constants of PZT-5H, see appendix A, have been chosen for all testing. The results are given in Tab. I and show a good agreement both for a number of element rings above two and also between the two methods. Both numerical solutions agree well with analytical results [14].

Furthermore discrete values of energy release rates are calculated along the crack front for the penny shaped crack, see Fig. 10.

In Fig. 13 the dependence of the energy release rate on the size of the integration domain is shown for the case of mechanical loading. The

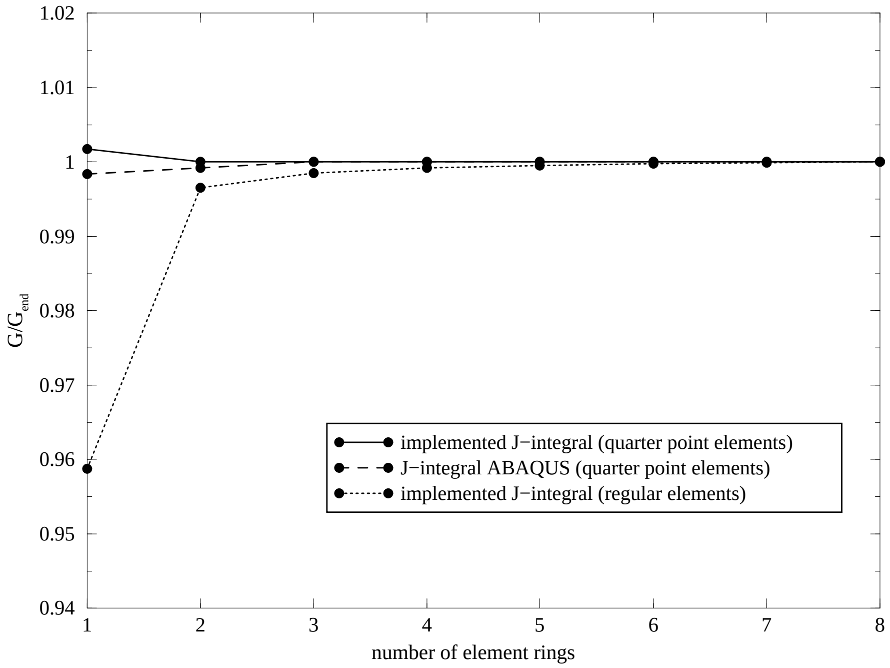

Figure 13. Convergence of the J–integral depending on the number of integration rings

values are normalized with respect to the value G_{end}, which is calculated with the largest integration domain (8 element rings). If regular crack front elements are used, a relative large domain (4 element rings) must be used to obtain a well converged result. Using quarter point elements leads to a better convergence. Then, just with two element rings a reasonable value for the mechanical energy release rate is calculated.

The commercial FEM-code ABAQUS provides a mechanical J–integral to analyze 3–dimensional crack configurations. Fig. 14 compares the mechanical part of the implemented J–integral with the ABAQUS J–integral. A fictitious material with the anisotropic mechanical characteristics of PZT–5H but without piezoelectric coupling was used for this comparison. Here, the deviations of the ABAQUS solution from the implemented method are shown. ABAQUS calculates energy release rates differing up to 1% from the implemented method in the middle of the crack front. However, the implemented J–integral delivers a more stable run of the curve.

For the case of a piezoelectric material under combined electromechanical loading, a comparison between the J–integral for the penny shaped crack, the CTE–method and the analytical solution was performed. The material poling axis is aligned perpendiculary to the crack

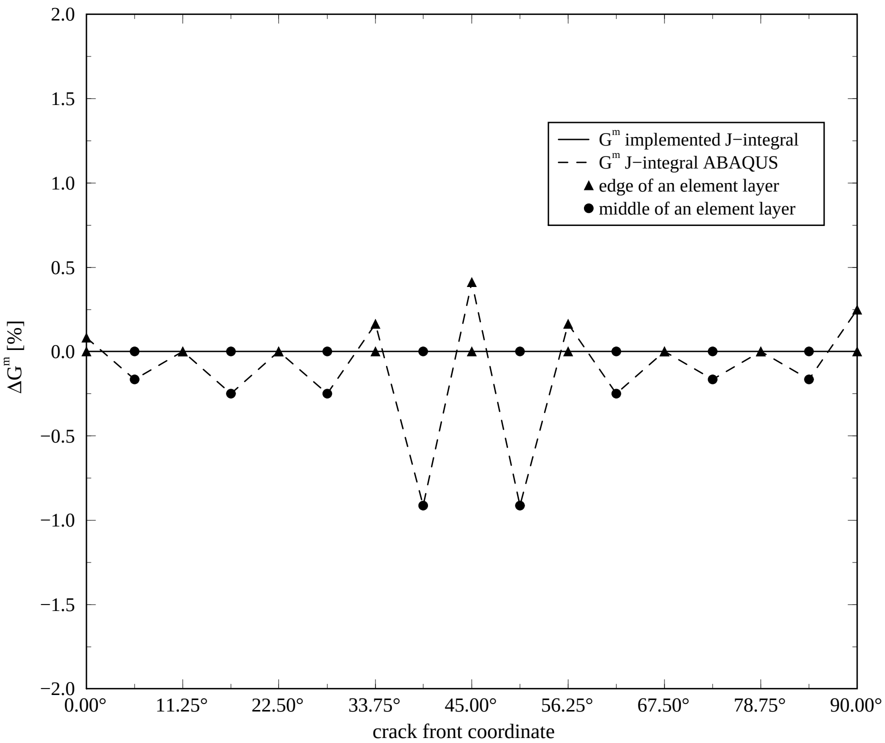

Figure 14. Implemented J–Integral and the ABAQUS J–integral in comparison

faces. As can be seen in Fig. 15, the J–integral provides an oscillating curve along the crack front. The results are normalized with respect to the analytical solution. Values calculated on points between two element layers exceed the values on points in the middle of an element layer by 0.5%. This difference is conditioned by the different shapes of the **q**–function (see Fig. 8) used on this points of the crack front. The CTE–method delivers values that are up to 3% higher than the analytical solution. The energy release rate is calculated from the K–factors using Eqn. (49). The CTE–method is based on the plain strain state, which hold true just for an infinite small surrounding of the crack front. The values used for calculating the intensity factors origin from nodes that have a finite distance to the crack front. According to general experiences [17], more exact results can be obtained by the CTE–method with reduced crack tip element size.

Finally, we compare the J–integral and CTE–method for the semi circular and quarter circular surface crack (see Fig. 16). Normalization is done with respect to the values of the implemented J–integral. Again

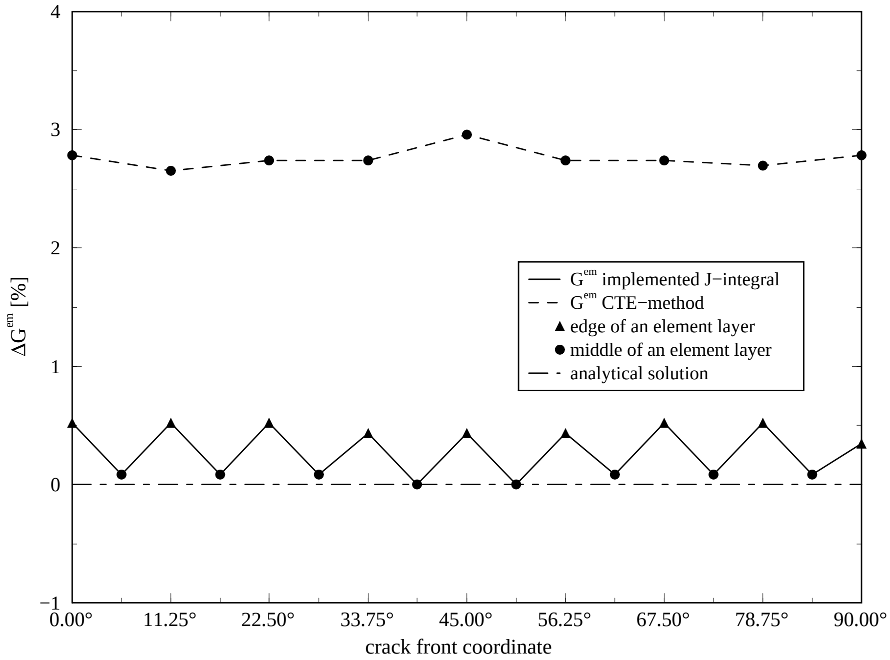

Figure 15. Electromechanical J–Integral and CTE–Method in comparison with the analytical solution

there are deviations between the results from both methods with a maximum amount of 3%.

6. Summary

A procedure for the numerical evaluation of the 3–dimensional (3–D) electromechanical J–integral has been presented. It allows the calculation of the electromechanical energy release rate along a spatial crack front of arbitrary shape in a piezoelectric body under combined electric and mechanical loading conditions. Thereby, values for nodal displacements and potentials as well as for stresses and electric displacements in the integration points are calculated from a FEM code. These results serve as input data for the computation of the J^{em}–integral.

The theory of the generalized J^{em}–integral has been derived for 2–D and 3–D applications. Like in the pure mechanical case, the J^{em}–integral yields a vector J_k^{em} for the 2–D formulation and a scalar quantity in the 3–D case. The path independence of the line (2–D) and surface (3–D) integral could be proved for vanishing stresses and electric charges on the crack faces, for absent body forces and volume

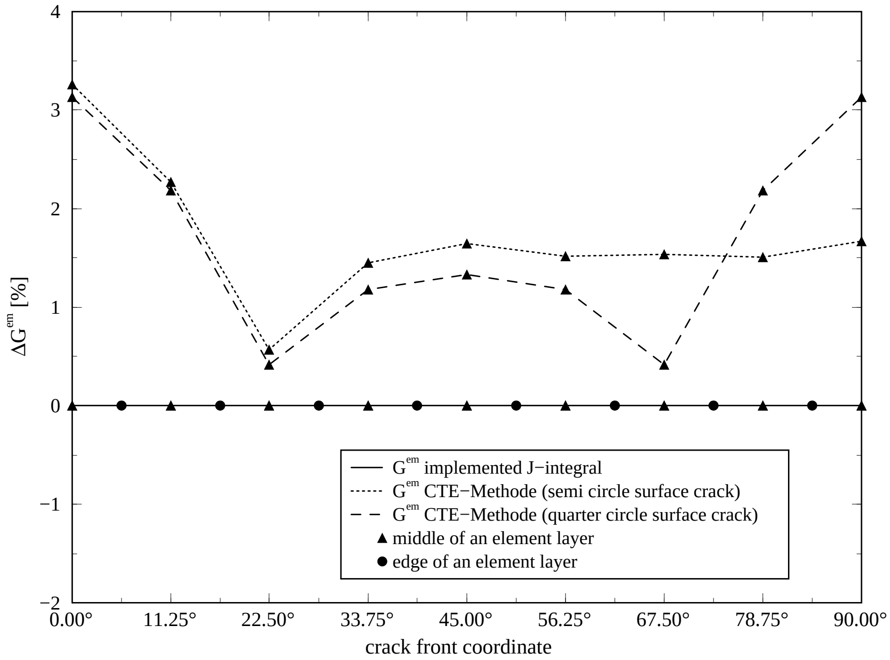

Figure 16. Electromechanical J–Integral and CTE–Method in comparision with the analytical solution

charges, as well as for uncurved crack faces, respectively. Furthermore, the theory of the electromechanical J–integral has been extended taking into account cracks in heterogeneous piezoelectric structures. The boundary integral is transformed into a domain integral using weighting functions q (2–D) and q_k (3–D), respectively. In contrast with the 2D formulation, the shape of the 3–dimensional weighting function requires the integration over the whole domain around the crack tip, exposed to a virtual displacement.

Exemplary calculations have been performed applying the domain integral formulation, neglecting body forces and volume charges as well as tractions and charges on the crack faces. The results show very good agreement with the analytical solution of the electromechanically loaded penny shaped crack. Best results were found using quarter point elements at the crack tip. A comparison with the commercial FEM code ABAQUS for elastic material, neglecting the piezoelectric coupling, showed a very good agreement of the local mechanical energy release rates, too. However, the course of the plot calculated from our J–integral implementation is smoother. A comparison with results from an alternative numerical method, the Crack Tip Element (CTE) method, showed deviations up to 3% using the same grid in both cases.

Better results can be obtained for the CTE method using a refined grid.

Acknowledgements

The authors gratefully acknowledge the German Research Foundation under contract Ku 929/3.

References

[1] Abaqus: 1995, 'ABAQUS Theory Manual'. Hibbitt, Karlsson & Sorensen, Inc. USA.

[2] Abendroth, M.: 2000, 'FEM-Implementierung des elektromechanischen J–Integrals zur räumlichen Analyse von Rissen in piezoelektrischen Strukturen'. *Diploma Thesis, TU Bergakademie Freiberg.*

[3] Chen, W. and T. Shioya: 1999, 'Fundamental solution for a penny shaped crack in a piezoelectric medium'. *Journal of the Mechanics and Physics of Solids 47* pp. 1459–1475.

[4] Cherepanov, G.: 1967, 'Rasprostranenie trechin v sploshnoi srede (About Crack Advance in the Continuum)'. *Prikladnaja Matematika i Mekhanica, 31* pp. 478–488.

[5] Eisentraut, U.: 1990, 'Bruchmechanische Analyse ebener und räumlicher thermoelastischer Rißprobleme mit der Methode der finiten Elemente'. Ph.D. thesis, Technische Universität "Otto von Guericke" Magdeburg, Fakultät für Technische Wissenschaften.

[6] Eshelby, J.: 1970, 'Energy relations and the energy momentum tensor in continuum mechanics'. *Inelastic Behavior of Solids edited by Kanninen, M.F. and others* pp. 77–114.

[7] Hellen, T.: 1975, 'On the method of virtual crack extensions'. *International Journal of Numerical Methods of Engineering 9* pp. 187–207.

[8] Kemmer, G. and H. Balke: 1997, 'Numerische Berechnung integraler Beanspruchungsgrößen bei Rissen in Piezokeramiken'. *ABAQUS-Anwendertreffen Innsbruck* pp. 18–26.

[9] Kuna, M.: 1995a, 'Ein Energiebilanzintegral für Risse in heterogenen Strukturen unter elektrischen und mechanischen Beanspruchungen'. *Proceedings, DVM–conference MICROMAT 1995 Berlin* pp. 341–348.

[10] Kuna, M.: 1995b, 'Energiebilanzintegrale für Risse in piezoelektrischen Werkstoffen unter elektrischen und mechanischen Beanspruchungen'. *Technische Mechanik, Band 15, Heft 3* pp. 195–204.

[11] Kuna, M.: 1998, 'Finite element analyses of crack problems in piezoelectric structures'. *Computational Materials Science 13* pp. 67–80.

[12] Moran, B. and C. Shih: 1987, 'Crack Tip and associated domain integrals from momentum and energy balance'. *Engineering Fracture Mechanics 27* pp. 615–642.

[13] Pak, Y.: 1990, 'Crack extension force in a piezoelectric material'. *Journal of Applied Mechanics 57* pp. 647–653.

[14] Pak, Y.: 1992, 'Linear electro-elastic fracture mechanics of piezoelectric materials'. *International Journal of Fracture 54* pp. 79–100.

[15] Park, S. and C. Sun: 1995, 'Effect of electric field on fracture of piezoelectric ceramic'. *International Journal of Fracture 70* pp. 202–216.

[16] Rice, J.: 1968, 'A path independent integral and the approximate analysis of strain concentration by notches and cracks'. *Journal of Applied Mechanics 35* pp. 379–386.

[17] Rossmanith, H.-P.: 1982, *Finite Elemente in der Bruchmechanik*. Wien–New York: Springer-Verlag.

[18] Shih, C., B. Moran, and T. Nakamura: 1986, 'Energy release rate along a three-dimensional crack front in a thermally stressed body'. *International Journal of Fracture 30* pp. 79–102.

[19] Shih, C., B. Moran, and T. Nakamura: 1988, 'Crack tip integrals and domain integral representation for three dimensional crack problems'. *AMD-Vol. 91, American Society of Mechanical Engineers.*

[20] Suo, Z., C. Kuo, D. Barnett, and J. Willis: 1992, 'Fracture mechanics for piezoelectric materials'. *Mechanics and Physics of Solids 40* pp. 739–765.

Appendix

A. Material constants of PZT-5H

The constitutive relations for PZT-5H [2, 11, 14] with the positive x_2–axis as poling axis can be written in contracted notations for the global coordinate system. The indices of the material constants $\bar{c}_{ij}$, $\bar{e}_{ij}$, $\bar{\kappa}_{ij}$ are notated with respect to the material axes, whereby x_3 corresponds to the poling axis.

$$\begin{bmatrix}\sigma_{11}\\ \sigma_{22}\\ \sigma_{33}\\ \sigma_{23}\\ \sigma_{31}\\ \sigma_{12}\end{bmatrix} = \begin{bmatrix}\bar{c}_{11} & \bar{c}_{13} & \bar{c}_{12} & 0 & 0 & 0\\ \bar{c}_{13} & \bar{c}_{33} & \bar{c}_{13} & 0 & 0 & 0\\ \bar{c}_{12} & \bar{c}_{13} & \bar{c}_{11} & 0 & 0 & 0\\ 0 & 0 & 0 & \bar{c}_{44} & 0 & 0\\ 0 & 0 & 0 & 0 & \frac{\bar{c}_{11}-\bar{c}_{12}}{2} & 0\\ 0 & 0 & 0 & 0 & 0 & \bar{c}_{44}\end{bmatrix} \begin{bmatrix}u_{1,1}\\ u_{2,2}\\ u_{3,3}\\ u_{2,3}\\ u_{3,1}\\ u_{1,2}\end{bmatrix} + \begin{bmatrix}0 & \bar{e}_{31} & 0\\ 0 & \bar{e}_{33} & 0\\ 0 & \bar{e}_{31} & 0\\ 0 & 0 & \bar{e}_{15}\\ 0 & 0 & 0\\ \bar{e}_{15} & 0 & 0\end{bmatrix} \begin{bmatrix}\phi_{,1}\\ \phi_{,2}\\ \phi_{,3}\end{bmatrix}$$

$$\begin{bmatrix}D_1\\ D_2\\ D_3\end{bmatrix} = \begin{bmatrix}0 & 0 & 0 & 0 & 0 & \bar{e}_{15}\\ \bar{e}_{31} & \bar{e}_{33} & \bar{e}_{31} & 0 & 0 & 0\\ 0 & 0 & 0 & \bar{e}_{15} & 0 & 0\end{bmatrix} \begin{bmatrix}u_{1,1}\\ u_{2,2}\\ u_{3,3}\\ u_{2,3}\\ u_{3,1}\\ u_{1,2}\end{bmatrix} - \begin{bmatrix}\bar{\kappa}_{11} & 0 & 0\\ 0 & \bar{\kappa}_{33} & 0\\ 0 & 0 & \bar{\kappa}_{11}\end{bmatrix} \begin{bmatrix}\phi_{,1}\\ \phi_{,2}\\ \phi_{,3}\end{bmatrix}$$

with the elastic constants [N/m^2]:

$$\begin{aligned}
\bar{c}_{11} &= 12.6 \cdot 10^{10} \\
\bar{c}_{12} &= 5.50 \cdot 10^{10} \\
\bar{c}_{13} &= 5.30 \cdot 10^{10} \\
\bar{c}_{33} &= 11.7 \cdot 10^{10} \\
\bar{c}_{44} &= 3.53 \cdot 10^{10}
\end{aligned}$$

the piezoelectric constants [C/m^2]:

$$\begin{aligned}
\bar{e}_{15} &= 17.0 \\
\bar{e}_{31} &= -6.5 \\
\bar{e}_{33} &= 23.3
\end{aligned}$$

and the dielectric constants [C/(Vm)]:

$$\begin{aligned}
\bar{\kappa}_{11} &= 1.51 \cdot 10^{-8} \\
\bar{\kappa}_{33} &= 1.30 \cdot 10^{-8}.
\end{aligned}$$

The relationships between the contracted and expanded notations are given as:

$$\begin{aligned}
\bar{C}_{1111} &= \bar{C}_{2222} = \bar{c}_{11} \\
\bar{C}_{1122} &= \bar{c}_{12} \\
\bar{C}_{1133} &= \bar{C}_{2233} = \bar{c}_{13} \\
\bar{C}_{2323} &= \bar{C}_{3131} = \bar{c}_{44} \\
\bar{C}_{3333} &= \bar{c}_{33} \\
\bar{C}_{1212} &= \frac{\bar{c}_{11} - \bar{c}_{12}}{2}
\end{aligned}$$

$$\begin{aligned}
\bar{e}_{113} &= \bar{e}_{323} = \bar{e}_{15} \\
\bar{e}_{311} &= \bar{e}_{322} = \bar{e}_{31} \\
\bar{e}_{333} &= \bar{e}_{33}.
\end{aligned}$$

The effective constants used for the Irwin matrix are given as:

$$\begin{aligned}
c_A &= 3.542 \cdot 10^{10} \text{ N/m}^2 \\
c_L &= 5.697 \cdot 10^{10} \text{ N/m}^2 \\
c_T &= 6.224 \cdot 10^{10} \text{ N/m}^2 \\
e &= 78.28 \text{ C/m}^2 \\
\kappa &= 2.184 \cdot 10^{-8} \text{ C/Vm}.
\end{aligned}$$

Address for Offprints:
Freiberg University of Mining and Technology
Institute of Mechanics and Fluid Dynamics
Lampadiusstraße 4, D-09596 Freiberg, Germany